Rotational spectrum of chloroform, "grass-roots among the forest of trees": The v2 = 1, v3 = 2, v5 = 1, and v6 = 3 vibrational states of CH35Cl3

Adina Ceausu-Velcescu, Petr Pracna, Laurent Margules, Adriana Predoi-Cross

Version of Record: https://www.sciencedirect.com/science/article/pii/S0022407321004295
Manuscript_7d2855030109e06a28482f68269bcbbb

Rotational spectrum of chloroform, "grass-roots among the forest of trees": The v_2=1, v_3=2, v_5=1, and v_6=3 vibrational states of $CH^{35}Cl_3$

Adina CEAUSU – VELCESCU*, Petr PRACNA†, Laurent MARGULES§,
Adriana PREDOI-CROSS[1,2]

*Université de Perpignan, LAMPS, 52 Avenue Paul Alduy, 66860 Perpignan Cedex, France

† University of Chemistry and Technology, Department of Analytical Chemistry, Technická 5, 166 28 Prague 6, Czech Republic

§ Université de Lille, CNRS, UMR8523-PhLAM, 59000 Lille, France

[1] Formerly at: Department of Physics and Astronomy, University of Lethbridge, Lethbridge AB, T1K 3M4 Canada; [2] Present address: Faculty of Science and Technology, Athabasca University,1 University Drive, Athabasca, AB, T9S 3A3, Canada

Proofs to: Dr. Adina CEAUSU-VELCESCU
Université de Perpignan,
LAMPS, 52 Avenue Paul Alduy, 66860 Perpignan Cedex France
Tel. (0033)4 68 66 22 19
Fax: (0033)4 68 66 22 34
E-mail address: adina@univ-perp.fr

Tables: 2

Figures: 7

Keywords: chloroform, high-resolution MMW spectroscopy, excited vibrational states, difference band

Abstract

We have recently analyzed the broadband millimeter-wave rotational spectrum of chloroform $CH^{35}Cl_3$ in the v_3=v_6=1 (E symmetry) and v_6=2 (A_1+E) vibrational excited. In the present work, we have used the same spectrum (recorded between 150-330 and 360-660 GHz) for a rotational analysis of the v_2=1 and v_3=2 A_1 states of the same molecule, together with a new analysis of the v_5=1 (E) fundamental vibration.

For the v_2=1 state (A_1, near 677 cm^{-1}), the body of assigned data comprises 392 rotational transitions. The corresponding frequencies were fitted within an isolated-level model, with a standard deviation of 36.4 kHz, and the obtained parameters are in good agreement with the previous IR work.

For the v_3=2 vibrational state (A_1, near 734 cm^{-1}), a total of 351 rotational transitions were assigned. Their fit was improved by inclusion of a second-order Coriolis coupling term with the v_5=1 fundamental level, providing standard deviation of 40.2 kHz.

At the same time, the description of the v_5=1 vibration (E symmetry, 776 cm^{-1}), studied previously with high-resolution as an isolated level, was also improved. The quantitative interpretation of the newly assigned 612 MMW data and the significantly extended set of IR assignments necessitated the introduction of the second-order Coriolis interaction with v_3=2, but more importantly of an anharmonic interaction with the v_6=3 (A_1+A_2+E, near 782 cm^{-1}) level. For this latter level more than 200 rotational transitions, together with several series of rovibrational transitions, could finally be assigned and included in the fit.

1. Introduction

The main purpose of the present work was to fully exploit the potential of the broadband rotational MMW spectroscopy and to prove that in a rotational spectrum, “grass-roots” still contain an interesting piece of information, among the “forest of trees” with which the analyses usually stop. Indeed, the millimeter-wave rotational spectrum of a small, heavy molecule, recorded using a natural sample, contains, besides the usually exploited information on the ground and low-lying excited states of the main isotopologues, some partly hidden, but still important information on higher excited states of the main species, and also on the ground state of minor isotopologues. However, this information is obviously also more difficult to extract and interpret.

The main isotopologue of chloroform, $CH^{35}Cl_3$, has several vibrational states below 800 cm^{-1} (Fig. 1), which could in principle be analyzed by rotational spectroscopy at room temperature. We have recently studied two such excited vibrational states, $v_3=v_6=1$ (627 cm^{-1}) and $v_6=2$ (520 cm^{-1}) [1]. For the former vibrational level, despite the extremely low intensity of its rotational lines, assignments were facilitated by its ‘isolated level’ character, and also by the great similarity with the $v_6=1$ rotational pattern. For the latter $v_6=2$ levels, however, situation was somewhat unprecedented. Indeed, these overtone levels, of A_1+E symmetry, are equally isolated from neighboring vibrational states, but their rotational pattern is quite complicated, as described in Ref. [1]. The intensity of the corresponding rotational lines, forming three distinct clusters, for $l_6=0$, $l_6=+2$ and $l_6=-2$ respectively, is however higher than that of the $v_3=v_6=1$ lines. Nevertheless, the effective B rotational constants, which determine the relative positions of the three clusters, are the result of the combined effects of a generalized, quasi-resonant, $l(2,2)$ interaction, relative positions of the unperturbed levels, together with centrifugal distortion.

The next vibrational level which provides weak, but still detectable spectroscopic patterns, is the $v_2=1$ level, at 676 cm^{-1}. The previous high-resolution IR study of the ν_2 band [2] provided spectroscopic constants which constitute a good basis for the current assignment of about 400 rotational transitions within this vibrational level.

Concerning the $v_3=2$ level (A_1 symmetry, at 734 cm^{-1}), a 1995 study by Carpenter *et al.* [3] has already published a few assignments of rotational lines within this level. We have equally to notice a 1999 study of the $2\nu_3$-ν_3 hot band, in the ν_3 region (near 367 cm^{-1}), by Pietila *et al.* [4]. Both these studies were a good starting point for the assignments, even though they

provided only the B and D_J rotational constants, which were used as initial values for the present work.

In the course of the analysis of the rotational transitions belonging to the v_3=2 level, it became necessary to consider its second-order Coriolis interaction with v_5=1. But this latter level is itself coupled to the v_6=3 (A_1+A_2+E) level through an anharmonic interaction. Therefore, an extended set of more than 4000 rovibrational transitions in the ν_5 fundamental band, together with 612 rotational transitions in the v_5=1 level, 26 rovibrational and 220 rotational transitions in the v_6=3 level, was merged to the 351 rotational transitions in v_3=2 in a global fit, including all the above-mentioned interactions.

Last, this work also gave us the opportunity of identifying a mysterious band, appearing at 510-515 cm^{-1}. This has been done in the course of the search for $3\nu_6$-ν_6 hot transitions; it became soon obvious that the regular spectral patterns observed in this region did not belong to the above-mentioned hot band, but to the ν_5-ν_6 difference band, as will be described later.

2. Experimental details

The rotational spectrum used in this work is that already employed in Ref. [1] for the rotational analysis of the v_3=v_6=1 and v_6=2 levels.

In addition, three infrared high-resolution spectra have been used in the present work, in order to collect rovibrational transitions pertaining to the ν_5, $3\nu_6$, and ν_5-ν_6 bands respectively. Two of them were recorded by Dr. V.-M. Horneman on an isotopically pure $CH^{35}Cl_3$ sample, using a Bruker IFS-120HR FTIR spectrometer, at the University of Oulu (Finland). The third spectrum was recorded at the CLS in Saskatoon (Canada), using a $CHCl_3$ sample with natural abundance.

The first spectrum (spectrum A), covering the 750-800 cm^{-1} spectral region, was recorded employing a Globar source, a KBr beamsplitter and a MCT96 detector. Sample pressure was of about 0.8 Pa, and about 0.93 Pa of OCS were introduced for calibration purposes. The spectrum was recorded with a 3.2-m optical pathlength and room temperature; the spectral resolution was of about 0.00125 cm^{-1}. Calibration was done using ν_1 OCS lines in the 812-890 cm^{-1} region [5][1]. Relative to these lines, the precision of our data is better than 5×10^{-5} cm^{-1}. The wavenumbers of the NIST report [5] were corrected by a multiplicative factor of 1.000 000 35, as suggested in the technical report of the IUPAC [6]. The recommended accuracy is better than 2.8×10^{-4} cm^{-1}.

[1] In Refs. [5], the band centered at 858.967 cm^{-1} is referred to as the ν_3 band.

The second spectrum (spectrum B) covers the 480-570 cm^{-1} spectral region and was recorded using a Globar source, a Mylar beamsplitter and a bolometer detector. The spectrum was recorded using a multipass cell, with a 41.8-m optical path length, at a pressure of 253 Pa and at room temperature. A total of 375 scans were co-added and the spectral resolution was of about 0.00125 cm^{-1}. Calibration was done with ν_2 OCS lines [7], OCS having been introduced in the multipass cell at a pressure of about 0.8 Pa. Relative to these lines, the precision of our data is better than 1×10^{-5} cm^{-1}. The accuracy was estimated to be 3×10^{-5} cm^{-1}.

The third spectrum (spectrum C) covers the 450-600 cm^{-1} spectral region and was recorded using the synchrotron radiation as a source at the Canadian Light Source in Canada, in a multipass cell with a 64-m optical path length, at a pressure of 400 Pa and at room temperature. A 6-micron Mylar beamsplitter and a Ge:Cu detector were employed, and the spectral resolution was 0.00096 cm^{-1}. The spectrum was calibrated using a few strong residual water lines present in the spectrum. The line positions of the water lines were taken from the HITRAN database. The line accuracy was estimated to be 1.0×10^{-4} cm^{-1}.

3. Rotational spectrum

The assignments of the rotational transitions were performed using the AABS package designed by Z. Kisiel for broadband rotational spectroscopy [8]. Intensity alternation due to nuclear spin statistics and Loomis-Wood representation of the spectrum in the AABS package were extremely helpful in progressive extension to higher J values.

3.1 The v_2=1 and v_3=2 rotational transitions

Assignment of the v_2=1 and v_3=2 rotational transitions was quite straightforward, despite their low intensity. The spectrum of $CH^{35}Cl_3$ in the region of J=35←34 transitions in the v_2=1 level is presented in Figure 2. The spectrum of the same isotopologue in the region of J=35←34 transitions in the v_3=2 and v_5=1 levels is plotted in Figure 3.

3.2 The v_5=1 rotational spectrum

The v_5=1 clusters of transitions were more difficult to assign, for several reasons: (i) their intensity, which is even lower than that of the above-mentioned bands; (ii) a partial overlap with v_3=2 and v_6=2 (l_6=0) clusters; (iii) last, but not least, the l_5=+1 and l_5= -1 clusters have almost identical B_{eff} values (as q_{22} is small and the separation of interacting levels is huge) and hence almost coincide (Fig. 3).

3.3 The v_6=3 rotational spectrum

The pattern of rotational transitions in the v_6=3 (A_1+A_2+E) level is again different from those of v_6=1 [9] and v_6=2 [1]. It is, however, again the l(2,2) resonance, connecting the (k-3, l_6=-3) ↔ (k-1, l_6=-1) ↔ (k+1, l_6=+1) ↔ (k+3, l_6=+3) levels, which mainly determines the B_{eff} values and the appearance of the four K-clusters of rotational lines, for a given value of J. This appearance can be easily understood by considering the case of an exact resonance, which concerns the $|\pm 1^{\pm 1}>$ and $|\pm 3^{\pm 3}>$ levels, each pair consisting of sublevels which are degenerate in the absence of the l(2,2) interaction. The Wang transformation yields two 2×2 blocks of A_+ and A_- levels:

$$A_{\pm} = \begin{pmatrix} E_1 \mp 4q_{22}J(J+1) & W(J,1) \\ W(J,1) & E_3 \end{pmatrix},$$

where $W(J,1) \simeq 2\sqrt{3}q_{22}\sqrt{J(J+1)-2}\sqrt{J(J+1)-6}$ and $E_3 - E_1 \simeq 8(C - B - 2C\zeta + g_{66}) \simeq 3222$MHz. The q_{22} interaction parameter is negative, which places the $|1^1, A_+>$ sublevel above the $|1^1, A_->$ one for all J values (situation which is similar to that encountered in a v_t=1 degenerate fundamental vibration). Also, the $|3^3, A_->$ sublevel is above the $|1^1, A_->$ one for all J values. The $|3^3, A_->$ sublevel is higher than $|1^1, A_+>$ for J<70; the two sublevels interchange their positions for $J > 71$. As a consequence of the effect of the l(2,2) interaction on the B_{eff} values, for low to moderate J-values, the lower and upper frequency clusters, which much resemble those of the v_6=1 state, are composed respectively of l_6=+1 transitions ('following' the (1^1, A_-, J+1)← (1^1, A_-, J) line) and l_6=-1 transitions ('following' the (1^1, A_+, J+1)← (1^1, A_+, J) line). These clusters are widely separated. The l_6=±3 clusters, starting from a common origin, lie inside this splitting and are much less separated.

The rotational transitions which could be safely assigned in the v_6=3 level are mainly k=l_6=±1 and k=l_6=±3 transitions, which are split by the l(2,2) interaction, as described above. The extreme weakness and the complex pattern of the four observed rotational clusters, for a given value of J, prevent us from a confident assignment of their K structure, except for J=22, 23, and 24.

4. Rovibrational spectrum

Assignments in the rovibrational spectra were performed with the aid of the interactive Loomis-Wood for Windows program [10] and checked, whenever possible, by lower state combination differences (LSCD).

4.1 The ν_5 fundamental band

This fundamental perpendicular band, centered at 776 cm^{-1} (Fig. 4), has been already given a detailed description in a previous high-resolution study [11]; its main characteristics will be therefore not recalled. The overview spectrum (Fig. 4) gives the location of the newly assigned subbands, as detailed in Section 5.

4.2 The ν_5-ν_6 difference band

This difference band, occurring in the 500-520 cm^{-1} region (Fig. 5), has already been mentioned by a 1995 paper by Fuβ and Weizbauer [12], but no assignment of its fine rotational structure has been undertaken by these authors. For such a difference band, both the lower and the upper vibrational levels are of E symmetry; two types of transitions are then allowed, corresponding respectively to the selection rules (Δk=0, Δl_5=−Δl_6=±1) and (Δk=∓1, Δl_5=Δl_6=±1) [13]. However, a simulation of the rotational structure according to the first set of selection rules and based on the already known rovibrational energies of the v_5=1 and v_6=1 levels, did not allow to obtain a reasonable agreement with the experimental spectrum. Indeed, the latter spectrum shows a series of quite intense, sharp peaks, regularly spaced by about 0.1 cm^{-1}. These structures become broader and partially resolved at lower wavenumbers. A closer inspection of these features revealed that they are not single lines, but rather composed of several, almost coincident, transitions with the selection rules Δk=∓1, Δl_5= Δl_6=±1. The spacing between these unresolved peaks, of 0.1 cm^{-1}, is due to a particular combination of constants C, $C\zeta_5$, and $C\zeta_6$; the separation between two ${}^pP_{K+1}(J+1)$ and ${}^pP_K(J)$ ($J \geq K$) adjacent lines is indeed roughly equal to $2(C + C\zeta_5 + C\zeta_6) \simeq 0.109\ \text{cm}^{-1} \simeq B_5$ (Fig. 6) which leads to a remarkable collapse of many individual lines into sharp peaks across the whole band and thus seemingly to an unexpectedly increased intensity of this difference band. Figure 6 presents a section of the spectrum of $CH^{35}Cl_3$ in the ν_5-ν_6 difference bands region. The progressions of ${}^pP_K(J=K+n)$ lines of the $\nu_5^{+1} - \nu_6^{-1}$ band are shown, with K and n values indicated on the figure. Each unresolved peak is composed of ${}^pP_K(J)$, ${}^pP_{K+2}(J+1)$, … lines, the spacing between two such lines being very weak, of $-4(C + C\zeta_5 + C\zeta_6) + 2B \simeq -0.0025$ cm^{-1}. We have to notice that, in principle, the same clustering phenomenon as that occurring for the ${}^pP_K(J)$, ${}^pP_{K+2}(J+1)$, … lines should also be observed for the ${}^rR_K(J)$, ${}^rR_{K+2}(J+1)$, … lines. However, the much lower intensity of the ΔJ=+1 side of the spectrum together with the wider spacing between adjacent lines make this clustering phenomenon less spectacular. Eventually, a total of 205 transitions belonging to 'special' series of ${}^pP_K(K+n)$ lines, n=0 to 15, as well as 273 ${}^pX_K(J)$ (X=P, Q; $-14 \leq K \cdot \Delta K \leq -4$) lines were included in the least-squares fit. The final

least-squares calculations also included 1539 lines of the above-mentioned difference band assigned from spectrum C where, despite the presence of two isotopologues of similar abundance, $CH^{35}Cl_3$ and $CH^{35}Cl_2{}^{37}Cl$, the main spectral features remained however those belonging to the first species[2]. Notice that, in these calculations, including the ν_5-ν_6 assigned rovibrational transitions, the v_6=1 parameters were all constrained to the values obtained in our v_6=1 previous study [14].

5. Results and discussion

The matrix elements of the rovibrational Hamiltonian used in the present work are detailed in Appendix A. Least-squares calculations were performed using the SIMFIT program, described in detail in Ref. [15].

5.1 The v_2=1 vibrational state

The ν_2 fundamental vibration (676.64 cm^{-1}) is well separated from the other vibrational states, the nearest vibration, $2\nu_3$, being almost 60 cm^{-1} higher. An isolated-level model could therefore be applied; a total of 392 rotational transitions, with $0 \le K \le 20$ and $22 \le J'' \le 77$, could be fitted, with a standard deviation of 36.4 kHz. Besides the B_2 rotational constant, we could also determine two quartic (D_J and D_{JK}) and two sextic (H_J and H_{JK}) centrifugal distortion parameters. The h_3 parameter of the Δk=6 interaction was also obtained, showing a remarkable consistency with the ground state value. The rotational parameters of this level, involved in equations (A1) and (A7) of the Appendix, are given in Table 1. The frequencies of the assigned transitions and their final reproduction are provided as Supplementary Material.

The good agreement observed between the B_2 value obtained in the present work and that obtained by Paso *et al.* [2] from the fit of ν_2 IR transitions shows that v_2=1 is (and can safely be treated as) an isolated level. Notice also that the present work reports the first assignment of rotational transitions in the v_2=1 vibrational state. Indeed, we can find in the literature a tentative assignment by Carpenter *et al.* [3] of about ten lines, for J''=17, which were thought as belonging to the v_2=1 state, owing to their intensity. These lines, obviously pertaining to a non-degenerate vibrational state, gave however a negative α_2^B value. We can now safely affirm that the lines reported in Table V of Ref. [3] are not ν_2 lines, but very likely (v_6=2, l_6=0) rotational transitions.

5.2 The v_3=2, v_5=1, and v_6=3 vibrational states

[2] This is presumably due to the fact that, for the $CH^{35}Cl_2{}^{37}Cl$ species, of C_s symmetry, each E degenerate vibrational mode splits into two modes, of *A'* and *A"* symmetry.

5.2.1. The v_3=2 level treated as isolated: Model I

The v_3=2 vibrational level (near 734 cm^{-1}) is also rather well separated from the next vibrational level, which is v_5=1 (776 cm^{-1}). The 351 assigned transitions ($0 \leq K \leq 20$ and $22 \leq J'' \leq 80$) could therefore be equally fitted to an isolated-level model (Model I, Table 1), with a standard deviation of 40.2 kHz, which is only slightly worse than that obtained for v_2=1. The B_{33} value obtained in this way is however quite different from that estimated using the B_0 value quoted in [14] together with the α_3^B value quoted in [4]: our 'isolated level' model allows obtaining B_{33}=3297.295 13(15) MHz, compared to $B_{33} = B_0 - 2\alpha_3^B =$ 3297.455 73(12) MHz. This important discrepancy indicates that some higher-order Coriolis interactions with neighboring levels were not considered.

5.2.2. Model II: a three-level interacting system

We have therefore elaborated a second model, in which $2v_3$ interacts with v_5 through a second-order Coriolis coupling ζ_{335}; the latter level is itself coupled to the $3v_6$ level (near 782 cm^{-1}) through an anharmonic (Darling-Dennison) term. In this model, the ζ_{335} term could not be refined, because the v_3=2 and v_5=1 levels do not cross; hence, ζ_{335} has been estimated as indicated in the Appendix of Ref. [16]. The harmonic and anharmonic contributions, calculated from force field parameters[3] kindly provided by J. Demaison [17], yield together ζ_{335}=0.013 382 cm^{-1}. When this second-order Coriolis coupling is introduced, the B_{33} value changes to 3297.424 98 (26) MHz, which is much closer to the above-mentioned prediction. Our second calculation included, besides the 351 rotational transitions in v_3=2, a total of 4326 rovibrational transitions pertaining to the v_5 band, as well as 612 rotational transitions in the v_5=1 vibrational state ($-32 \leq K \cdot l \leq 20$ and $22 \leq J \leq 69$). Concerning the v_5 infrared band, the data set has been enriched with respect to that used in the previous study [11] by the inclusion of the ${}^pX_{26\text{-}39}$ series ($X = P, Q$), around the anharmonic resonance crossings with (v_6=3, l_6= -1).

In Figure 7 we have plotted the reduced energies (pure J-dependent terms not included) against J, for the v_5=1^{-1} and v_6=3^{-1} levels. The locations of resonant crossings due to Darling-Dennison interaction are marked. Thanks to a large variety of crossings, shown on Fig. 7, the anharmonic resonance parameter k_{5666} was thus obtained with reasonably good accuracy, 2429.031 (37) MHz. Moreover, 26 infrared transitions belonging to the $3\nu_6^{\pm 1}$ band ($K''\cdot\Delta K$= -57 and -58), together with 220 rotational transitions in the v_6=3 level could be assigned and fitted. The v_5 IR data eventually included rovibrational transitions with $-39 \leq K'' \cdot \Delta K \leq 57$

[3] These calculations were performed at the MP2/TZ2Pf level.

and $0 \leq J'' \leq 84$. Among them, we have also introduced the ${}^{r}Q_0$ and ${}^{r}R_0$ branches (not included in the global fit of the previous study [11]), which provide the main information on the $l(2,2)$ interaction parameters. The body of data eventually included about 2000 rovibrational transitions of the $\nu_5^{\pm 1} - \nu_6^{\mp 1}$ difference band, assigned on the two FTIR spectra we had at our disposal (spectra B and C). The results of our Model II, including also eight fitted diagonal parameters of the $v_6=3^{\pm 1}$ sublevel and four of the $v_6=3^{\pm 3}$ sublevel (the bandcenter, the B rotational constant, the D_J and D_{JK} quartic centrifugal distortion parameters), together with the q_{22}, f_{22}^{J}, and q_{12}^{l} parameters, are listed in Table 2. The frequencies/wavenumbers of the assigned rotational/rovibrational transitions as well as their final reproduction are provided as Supplementary Material.

It would be also interesting to compare certain parameters of the $v_5=1$, redetermined in our work, with previous experimental determinations [11] and also with force field calculations [17]. For instance, from $C\zeta_5$=1425.633 3 (70) MHz and C_5=1708.402 57 (73) MHz, we obtain a Coriolis coupling ζ_5=0.834 483 (4), which agrees with ζ_5=0.833 82 (10) obtained in Ref. [11] within 5σ, but is quite different from the force field calculations, ζ_5=0.853 9. Situation is similar for the main $l(2,2)$ interaction parameter: we obtain q_{22}= -2.332 19 (35)×10^{-5} cm^{-1}, whereas Ref. [11] gives -2.47 (2)×10^{-5} cm^{-1} and the anharmonic force field calculations [17], -1.75×10^{-5} cm^{-1}.

Supplementary data associated with this article can be found in the online version, at doi: …

6. Conclusion

The present study, dealing with the rotational spectrum of $CH^{35}Cl_3$ in the $v_2=1$, $v_3=2$, $v_5=1$, and $v_6=3$ vibrational excited states, demonstrates once again that a very large amount of information can be collected from a millimeter-wave spectrum. This information concerns, besides the ground state and lower excited states of main isotopologues, higher excited states and also ground state of minor isotopologues [18]. The assignment of several hundreds of, often very weak, rotational transitions for these excited states thus allows a very accurate determination of rotational and centrifugal distortion constants (quartic and sextic), as well as rovibrational interaction parameters. Last, but not least, the most complete knowledge of the rovibrational parameters of a molecule is achieved, whenever possible, by combining rotational and rovibrational data in a merged least-squares fit. This has been done in the present study for the ν_5 fundamental vibration of chloroform.

Acknowledgments

The authors would like to thank Dr. V.-M. Horneman from the University of Oulu (Finland) for providing them the FTIR spectra A and B used in the present work. Dr. J. Demaison from the University of Lille (France) is also greatly acknowledged for providing some, unpublished, force field calculations. We thank Dr. B. Billinghurst for recoding the chloroform spectra at the Canadian Light Source, a national research facility of the University of Saskatchewan, which is supported by the Canada Foundation for Innovation (CFI), the Natural Sciences and Engineering Research Council (NSERC), the National Research Council (NRC), the Canadian Institutes of Health Research (CIHR), the Government of Saskatchewan, and the University of Saskatchewan.

Appendix A. Definition of the matrix elements of the effective vibration-rotational Hamiltonian

The diagonal matrix elements were defined conventionally as

$$E_{vr}(J,k,l_t) = E_v + B_v J(J+1) + (C_v - B_v)k^2 - D_J^v J^2(J+1)^2 - D_{JK}^v J(J+1)k^2$$
$$-D_K^v k^4 + H_J^v J^3(J+1)^3 + H_{JK}^v J^2(J+1)^2 k^2 + H_{KJ}^v J(J+1)k^4 + H_K^v k^6$$
$$+L_J^v J^4(J+1)^4 + L_{JJK}^v J^3(J+1)^3 k^2 + L_{JK}^v J^2(J+1)^2 k^4 + L_{JKK}^v J(J+1)k^6 + L_K^v k^8$$
$$+\left[-2(C\zeta_t)_v + \eta_{tJ}J(J+1) + \eta_{tK}k^2 + \tau_{tJ}J^2(J+1)^2 + \tau_{tJK}J(J+1)k^2 + \tau_{tK}k^4\right.$$
$$\left.+\sigma_{tJ}J^3(J+1)^3 + \sigma_{tJK}J^2(J+1)^2k^2 + \sigma_{tKJ}J(J+1)k^4 + \sigma_{tK}k^6\right]kl_t \quad \text{(A1)}$$

The following off-diagonal matrix elements were considered

a) l-type operators

$$\left\langle v_t^{l_t\pm2}; J, k\pm2\middle|\mathbf{H}_{22}+\mathbf{H}_{24}+\mathbf{H}_{26}\middle|v_t^{l_t}; J, k\right\rangle$$
$$= [(v_t \mp l_t)(v_t \pm l_t + 2)]^{1/2}\left\{q_{22} + f_{22}^J J(J+1) + f_{22}^K[k^2 + (k\pm2)^2]\right.$$
$$\left.+f_{22}^{JJ}J^2(J+1)^2 + f_{22}^{JK}J(J+1)[k^2+(k\pm2)^2] + f_{22}^{KK}[k^4+(k\pm2)^4]\right\}F_2^{\pm}(J,k) \quad \text{(A2)}$$

$$\left\langle v_t^{l_t\pm2}; J, k\mp1\middle|\mathbf{H}_{22}+\mathbf{H}_{24}\middle|v_t^{l_t}; J, k\right\rangle = [(v_t \mp l_t)(v_t \pm l_t + 2)]^{1/2}$$
$$\times\left\{\left[q_{12} + f_{12}^J J(J+1)\right](2k\mp1) + f_{12}^K[k^3 + (k\mp1)^3]\right\}F_1^{\mp}(J,k) \quad \text{(A3)}$$

$$\left\langle v_t^{l_t\pm2}; J, k\mp1\middle|\mathbf{H}_{41}+\mathbf{H}_{43}\middle|v_t^{l_t}; J, k\right\rangle = [(v_t \mp l_t)(v_t \pm l_t + 2)]^{1/2}$$
$$\times\left\{q_{12}^l + f_{12}^{lJ}J(J+1) + f_{12}^{lK}[k^2 + (k\mp1)^2]\right\}(2l_t \pm 2)F_1^{\mp}(J,k) \quad \text{(A4)}$$

$$\left\langle v_t^{l_t\pm2}; J, k\mp4\middle|\mathbf{H}_{24}+\mathbf{H}_{26}\middle|v_t^{l_t}; J, k\right\rangle = [(v_t \mp l_t)(v_t \pm l_t + 2)]^{1/2}$$
$$\times\left\{f_{42} + f_{42}^J J(J+1) + f_{42}^K[k^2 + (k\mp4)^2]\right\}F_4^{\mp}(J,k) \quad \text{(A5)}$$

b) Δk=±3 operator

$$\left\langle v_t^{l_t}; J, k\pm3\middle|\mathbf{H}_{23}+\mathbf{H}_{25}\middle|v_t^{l_t}; J, k\right\rangle = \left\{d_t + d_t^J J(J+1) + d_t^K[k^2 + (k\pm3)^2]\right\}l_t F_3^{\pm}(J,k) \quad \text{(A6)}$$

c) Δk=±6 operator

$$\left\langle v_t^{l_t}; J, k\pm6\middle|\mathbf{H}_{06}+\mathbf{H}_{08}\middle|v_t^{l_t}; J, k\right\rangle = \left\{h_3 + h_3^J J(J+1) + h_3^K[k^2 + (k\pm6)^2]\right\}F_6^{\pm}(J,k) \quad \text{(A7)}$$

The notation of the matrix elements of the rotational shifting operators was taken as

$$F_n^{\pm}(J,k) = \prod_{i=1}^{n}[J(J+1) - (k\pm i\mp1)(k\pm i)]^{1/2} \quad \text{(A8)}$$

Besides these usual intra-vibrational off-diagonal operators, the following ones, describing inter-vibrational interactions in the $2\nu_3/\nu_5/3\nu_6$ system, were considered. In the following

equations, the $L_n^{\pm}$ and $L_{t\pm}^{\pm}$ operators (the lower and the upper signs are independent) are respectively vibrational ladder and double ladder operators, as defined for instance in Ref. [19].

a) Second-order Coriolis interaction $2\nu_3/\nu_5$

$\mathbf{H}_{31} = \frac{1}{4}\zeta_{nnt}L_n^-L_n^-(L_{t+}^+J_- - L_{t-}^+J_+) + h.c.$, where n=3 and t=5. Matrix elements:

$$\langle 0, 1^{\pm 1}; J, k \pm 1|\mathbf{H}_{31}|2, 0^0; J, k\rangle = \pm\frac{1}{\sqrt{2}}\zeta_{335}F_1^{\pm}(J, k) \quad \text{(A9)}$$

b) Darling-Dennison interaction $\nu_5^{\pm 1}/3\nu_6^{\pm 1}$

$\mathbf{H}_{40} = k_{5666}(L_{t+}^+L_{t\prime-}^-L_{t\prime+}^-L_{t\prime-}^- + L_{t-}^+L_{t\prime+}^-L_{t\prime-}^-L_{t\prime+}^-) + h.c.$, where t=5 and t'=6. Matrix elements:

$$\langle 1^{\pm 1}, 0^0; J, k|\mathbf{H}_{40}|0^0, 3^{\pm 1}; J, k\rangle = \sqrt{2}k_{5666} \quad \text{(A10)}$$

c) Δk=±1, Δl=∓2 interactions

i. $\nu_5^{\mp 1}/3\nu_6^{\mp 3}$: $\mathbf{H}_{41}^a = f_{41}^a(L_{t+}^-L_{t\prime-}^+L_{t\prime-}^+L_{t\prime-}^+J_- - L_{t-}^-L_{t\prime+}^+L_{t\prime+}^+L_{t\prime+}^+J_+) + h.c.$ Matrix elements:

$$\langle 0^0, 3^{\mp 3}; J, k \pm 1\big|\mathbf{H}_{41}^a\big|1^{\mp 1}, 0^0; J, k\rangle = \pm\sqrt{6}f_{41}^aF_1^{\pm}(J, k) \quad \text{(A11)}$$

ii. $\nu_5^{\pm 1}/3\nu_6^{\mp 1}$: $\mathbf{H}_{41}^b = f_{41}^b(L_{t-}^-L_{t\prime+}^+L_{t\prime-}^+L_{t\prime-}^+J_- - L_{t+}^-L_{t\prime-}^+L_{t\prime+}^+L_{t\prime+}^+J_+) + h.c.$ Matrix elements:

$$\langle 0^0, 3^{\mp 1}; J, k \pm 1\big|\mathbf{H}_{41}^b|1^{\pm 1}, 0^0; J, k\rangle = \pm\sqrt{2}f_{41}^bF_1^{\pm}(J, k) \quad \text{(A12)}$$

d) Δk=Δl=±2 interactions

i. $\nu_5^{\mp 1}/3\nu_6^{\mp 3}$: $\mathbf{H}_{42}^a = f_{42}^a(L_{t+}^-L_{t\prime-}^+L_{t\prime-}^+L_{t\prime-}^+J_+^2 + L_{t-}^-L_{t\prime+}^+L_{t\prime+}^+L_{t\prime+}^+J_-^2) + h.c.$ Matrix elements:

$$\langle 0^0, 3^{\mp 3}; J, k \mp 2\big|\mathbf{H}_{42}^a\big|1^{\mp 1}, 0^0; J, k\rangle = \sqrt{6}f_{42}^aF_2^{\mp}(J, k) \quad \text{(A13)}$$

ii. $\nu_5^{\pm 1}/3\nu_6^{\mp 1}$: $\mathbf{H}_{42}^b = f_{42}^b(L_{t-}^-L_{t\prime+}^+L_{t\prime-}^+L_{t\prime-}^+J_+^2 + L_{t+}^-L_{t\prime-}^+L_{t\prime+}^+L_{t\prime+}^+J_-^2) + h.c.$ Matrix elements:

$$\langle 0^0, 3^{\mp 1}; J, k \mp 2\big|\mathbf{H}_{42}^b|1^{\pm 1}, 0^0; J, k\rangle = \sqrt{2}f_{42}^bF_2^{\mp}(J, k) \quad \text{(A14)}$$

Figure captions

Figure 1. Level diagram of the lowest vibrational states of $CH^{35}Cl_3$ up to 800 cm^{-1}, out of which the cluster of the four highest energy vibrational states (those above the dotted horizontal line) were analyzed in the current study. All energy values are in cm^{-1} units.

Figure 2. The rotational spectrum of chloroform in the region of J=35←34 transitions in the v_2=1 level of the $CH^{35}Cl_3$ isotopologue. Upper panel: experimental spectrum (natural sample; spectral range, 150-330 GHz; pressure, 30 Pa; pathlength, 2.2 m; room temperature). Lower panel: simulated spectrum, with several K-assignments indicated. The pointer and the dotted horizontal line indicate the position of the K=0 transition (with its upper and lower state quantum numbers given below the corresponding labels).

Figure 3. The rotational spectrum of chloroform in the region of J=35←34 transitions in the v_3=2 and v_5=1 levels of the $CH^{35}Cl_3$ isotopologue. Upper panel: experimental spectrum (same conditions as for Figure 2). Lower panel: simulated spectrum, with several K-assignments for v_3=2 and k^l-assignments for v_5=1 indicated. Transitions in the v_3=2 level are in black, those in the v_5=1 level in blue. The pointer and the dotted horizontal line indicate the position of the K=0 transition in v_3=2 (with its upper and lower state quantum numbers given below the corresponding labels).

Figure 4. Overview of the 760-790 cm^{-1} region of the infrared spectrum of $CH^{35}Cl_3$, with the bandcenters of ν_5, $3\nu_6^{\pm 1}$, and $3\nu_6^{\pm 3}$, as well as the newly assigned sections, denoted. Experimental conditions: $CH^{35}Cl_3$ sample; pressure, 0.8 Pa; optical pathlength, 3.2 m; room temperature.

Figure 5. Overview of the 495-530 cm^{-1} region of the infrared spectrum of $CH^{35}Cl_3$, showing the $\nu_5^{\pm 1} - \nu_6^{\mp 1}$ difference band, with section shown in the subsequent Figure 6 marked. Experimental conditions: natural sample; pressure, 400 Pa; optical pathlength, 64 m; room temperature. The sharp, intense lines marked by an asterisk are water lines and were used for calibration.

Figure 6. Detail of the infrared spectrum of $CH^{35}Cl_3$ in the v_5-v_6 difference bands region; several clear progressions of ${}^pP_K(J=K+n)$ lines of the $\nu_5^{+1} - \nu_6^{-1}$ band are shown, with K and n values indicated. Upper panel: experimental spectrum ($CH^{35}Cl_3$ sample; pressure, 253 Pa; optical pathlength, 41.8 m; room temperature). Lower panel: simulated spectrum. The very

sharp lines marked by an asterisk belong to the ν_2 band of the OCS molecule, added to the $CH^{35}Cl_3$ sample for calibration purposes (pressure of OCS of about 0.8 Pa).

Figure 7. Reduced energies (pure *J*-dependent terms not included) against *J*, for the $v_5=1^{-1}$ (red circles) and $v_6=3^{-1}$ (blue circles) levels. Positions of resonant crossings due to Darling-Dennison interaction are indicated.

Table captions

Table 1. Molecular parameters of the $v_2=1$ and $v_3=2$ levels (Model I) of $CH^{35}Cl_3$.

Table 2. Molecular parameters of the $v_3=2$, $v_5=1$, and $v_6=3$ levels of $CH^{35}Cl_3$ (Model II).

References

1 A. Ceausu-Velcescu, P. Pracna, R. A. Motiyenko, L. Margulès, Rotational spectroscopy in the ν_3=ν_6=1 and ν_6=2 vibrational states of $CH^{35}Cl_3$, J Quant Spectrosc Radiat Transf 250; 2020: 107006.

2 R. Paso, V.-M. Horneman, J. Pietilä, R. Anttila, High-resolution study of the infrared band ν_2 of $CH^{35}Cl_3$, Chem Phys Lett 247; 1995: 277-82.

3 J. H. Carpenter, P. J. Seo, D. H. Whiffen, The rotational spectrum of chloroform in its ground and excited vibrational states, J Mol Spectrosc 170; 1995: 215-27.

4 J. Pietilä, V.-M. Horneman, R. Anttila, High-resolution infrared study of the parallel band ν_3 of chloroform $CH^{35}Cl_3$, Mol Phys 96; 1999: 1449-56.

5 A. G. Maki, J. S. Wells, Wavenumber calibration tables from heterodyne frequency measurements, technical Report NIST Special Publication 821, US Department of Commerce, December 1991; A. G. Maki, J. S. Wells, New wavenumber calibration tables from heterodyne frequency measurements, J Res Natl Inst Stand Technol 97; 1992: 409-70.

6 G. Guelachvili, M. Birk, Ch. J. Bordé, J. W. Brault, L. R. Brown, B. Carli, A. R. H. Cole, K. M. Evenson, A. Fayt, D. Hausamann, J. W. C. Johns, J. Kauppinen, Q. Kou, A. G. Maki, K. Narahari Rao, R. A. Toth, W. Urban, A. Valentin, J. Vergès, G. Wagner, M. H. Wappelhorst, J. S. Wells, B. P. Winnewisser, M. Winnewisser, High resolution wavenumber standards for the infrared, Pure Appl Chem 68; 1996: 193–208; J Mol Spectrosc 177; 1996: 164 –79; Spectrochim Acta A52; 1996: 717–32.

7 V.-M. Horneman, Improved wave-number tables of the carbonyl sulfide ν_2 and $2\nu_2$ bands and guides for accurate measurement, J Opt Soc Am B 21; 2004: 1050-64.

8 Z. Kisiel in: J. Demaison *et al.* (Eds.), "Spectroscopy from Space", Kluwer Academic Publishers, Dordrecht, 2001, p. 91-106; http://info.ifpan.edu.pl./~kisiel/prospe.htm.

9 L. Margulès, J. Demaison, P. Pracna, Rotational spectrum in the ν_6=1 and ν_3=1 levels of chloroform, J Mol Struct 795; 2006: 157-62.

10 W. Lodyga, M. Kreglewski, P. Pracna, Š. Urban, Advanced graphical software for assignments of transitions in rovibrational spectra, J Mol Spectrosc 243; 2007: 182-8.

11 J. Pietilä, V.-M. Horneman, R. Anttila, B. Lemoine, F. Reynaud, J.-M. Colmont, The perpendicular fundamental ν_5 of chloroform $^{12}CH^{35}Cl_3$: high resolution infrared study of the ν_5 band together with the millimetre-wave rotational spectrum, Mol Phys 98; 2000: 549-57.

12 W. Fuβ and S. Weizbauer, Anharmonische Konstanten von $SiHCl_3$ und $CHCl_3$, Ber. Bunsenges. Phys. Chem. 99; 1995: 289-95.

13 G. Tarrago, O. N. Ulenikov, G. Poussigue, Dipole moment matrix for vibration-rotation transitions in C_{3v} molecules, J Phys 45; 1984: 1429-47.

14 P. Pracna, A. Ceausu-Velcescu, V.-M. Horneman, The ground and ν_6=1 vibrational levels of $HC^{35}Cl_3$: The first high-resolution analysis of the ν_6 fundamental band, J Quant Spectrosc Rad Transf 113; 2012: 1220-5.

15 P. Pracna, J. Demaison, G. Wlodarczak, A.G. Lesarri, G. Graner, Simultaneous analysis of rovibrational and rotational spectra of the ν_5=1 and ν_8=1 vibrational levels of propyne, J Mol Spectrosc 177; 1996: 124-33.

16 J. Cosléou, J. Demaison, K. Sarka, W. Thiel, Ab initio anharmonic force field, molecular parameters, equilibrium structure and enthalpy of formation of fluoroform, Mol Phys 102; 2004: 1827-41.

17 J. Demaison, private communication.

18 J.-M. Colmont, D. Priem, P. Dréan, J. Demaison, James E. Boggs, Rotational spectra of the isotopic species of chloroform: experimental and ab initio structures, J Mol Spectrosc 191; 1998: 158-75.

19 K. Sarka, L. Nová Stříteská, A. Ceausu-Velcescu, Effective Hamiltonians for the Fermi resonance – interacting states of C_{3v} molecules, J Mol Spectrosc 311; 2015: 84-99.

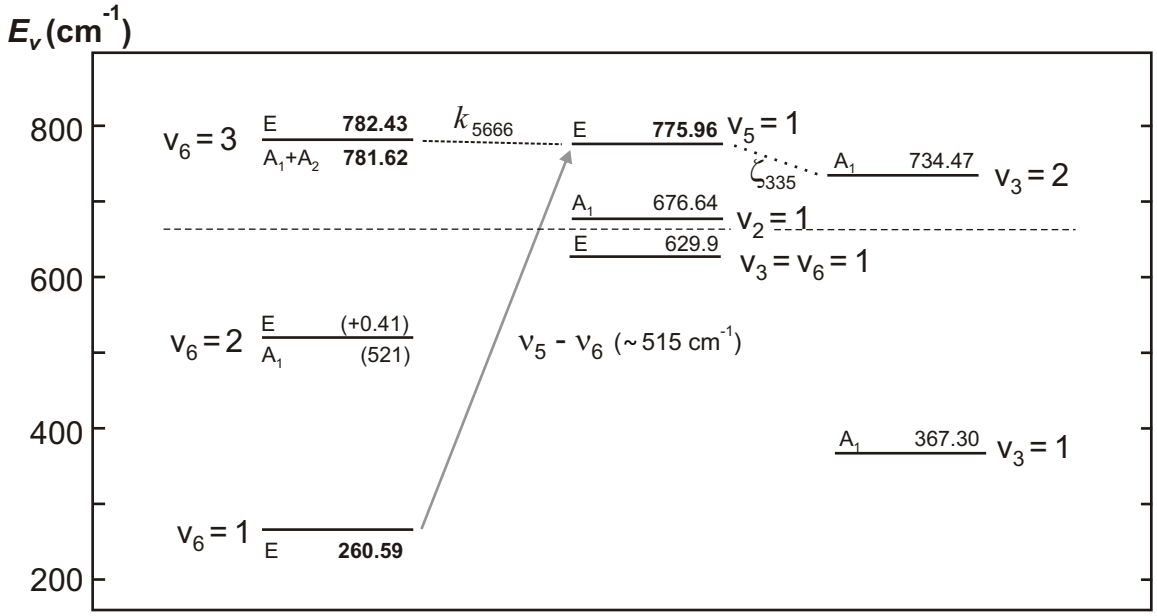
E_v (cm^{-1})
800
600
400
200
$v_6 = 3$
E 782.43
A_1+A_2 781.62
k_{5666}
E 775.96
$v_5 = 1$
ζ_{335}
A_1 734.47
$v_3 = 2$
A_1 676.64
$v_2 = 1$
E 629.9
$v_3 = v_6 = 1$
$v_6 = 2$
E (+0.41)
A_1 (521)
$\nu_5 - \nu_6$ (~ 515 cm^{-1})
A_1 367.30
$v_3 = 1$
$v_6 = 1$
E 260.59

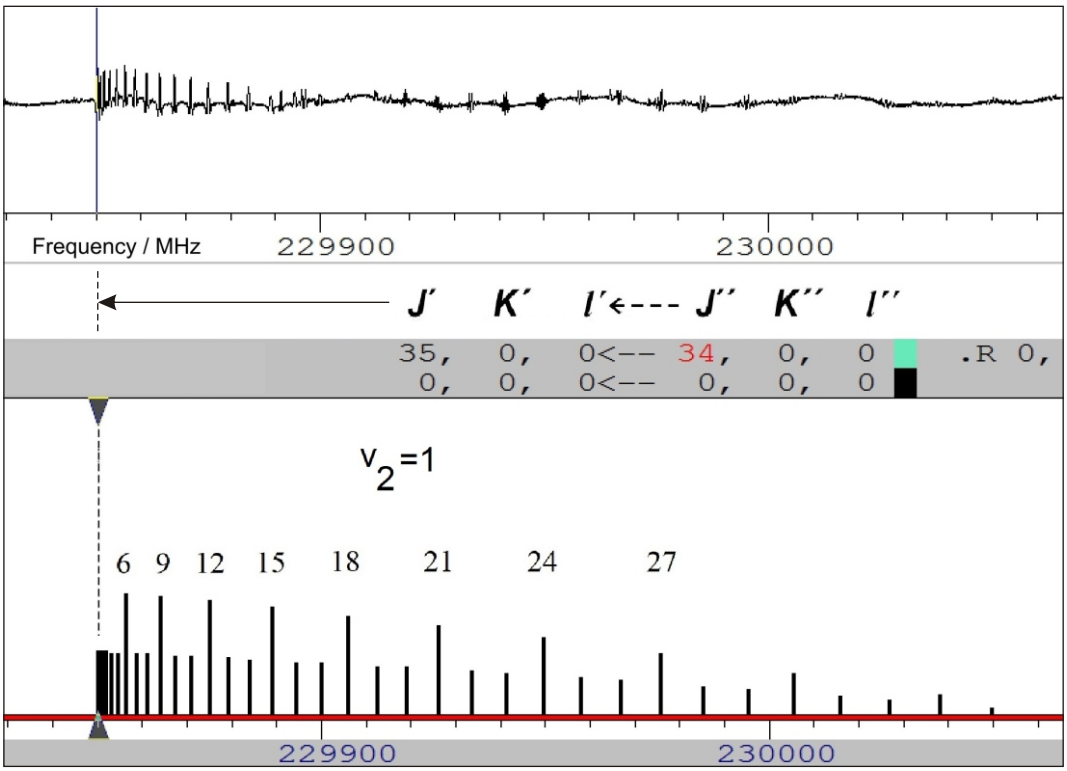
Frequency / MHz
229900
230000
J′ K′ l′←--- J′′ K′′ l′′
35, 0, 0<-- 34, 0, 0 .R 0,
0, 0, 0<-- 0, 0, 0
v2=1
6 9 12 15 18 21 24 27
229900
230000

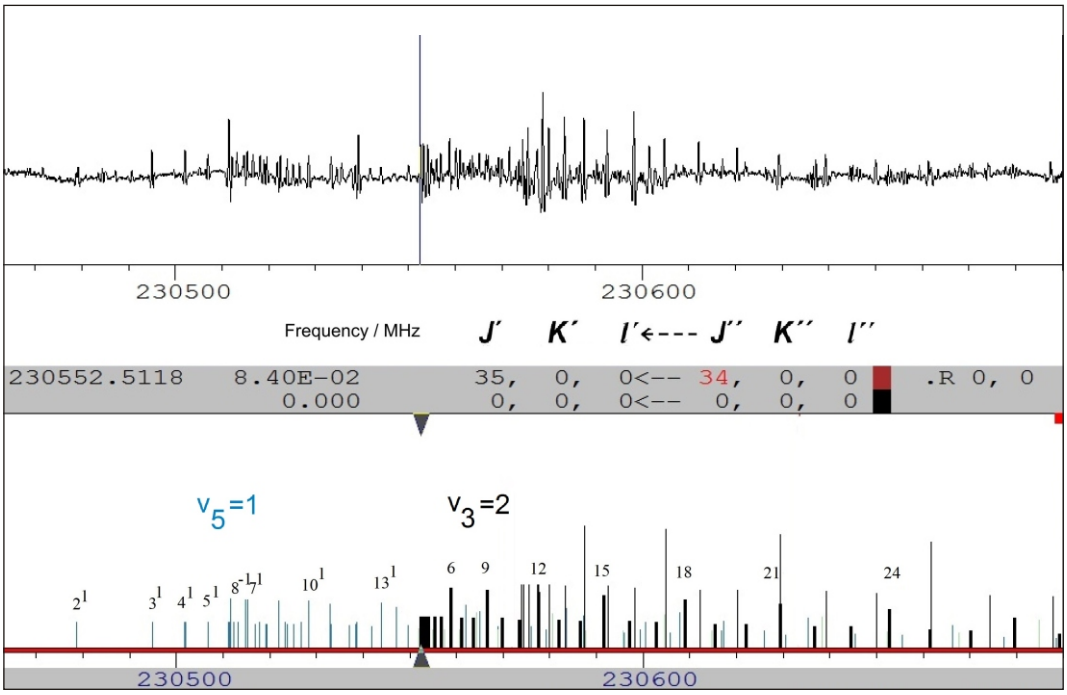
230500
230600
Frequency / MHz
J′ K′ l′←--- J′′ K′′ l′′
230552.5118 8.40E-02 35, 0, 0<-- 34, 0, 0 .R 0, 0
0.000 0, 0, 0<-- 0, 0, 0
v5=1
v3=2
2^1
3^1
4^1
5^1
8^-1 7^1
10^1
13^1
6
9
12
15
18
21
24
230500
230600

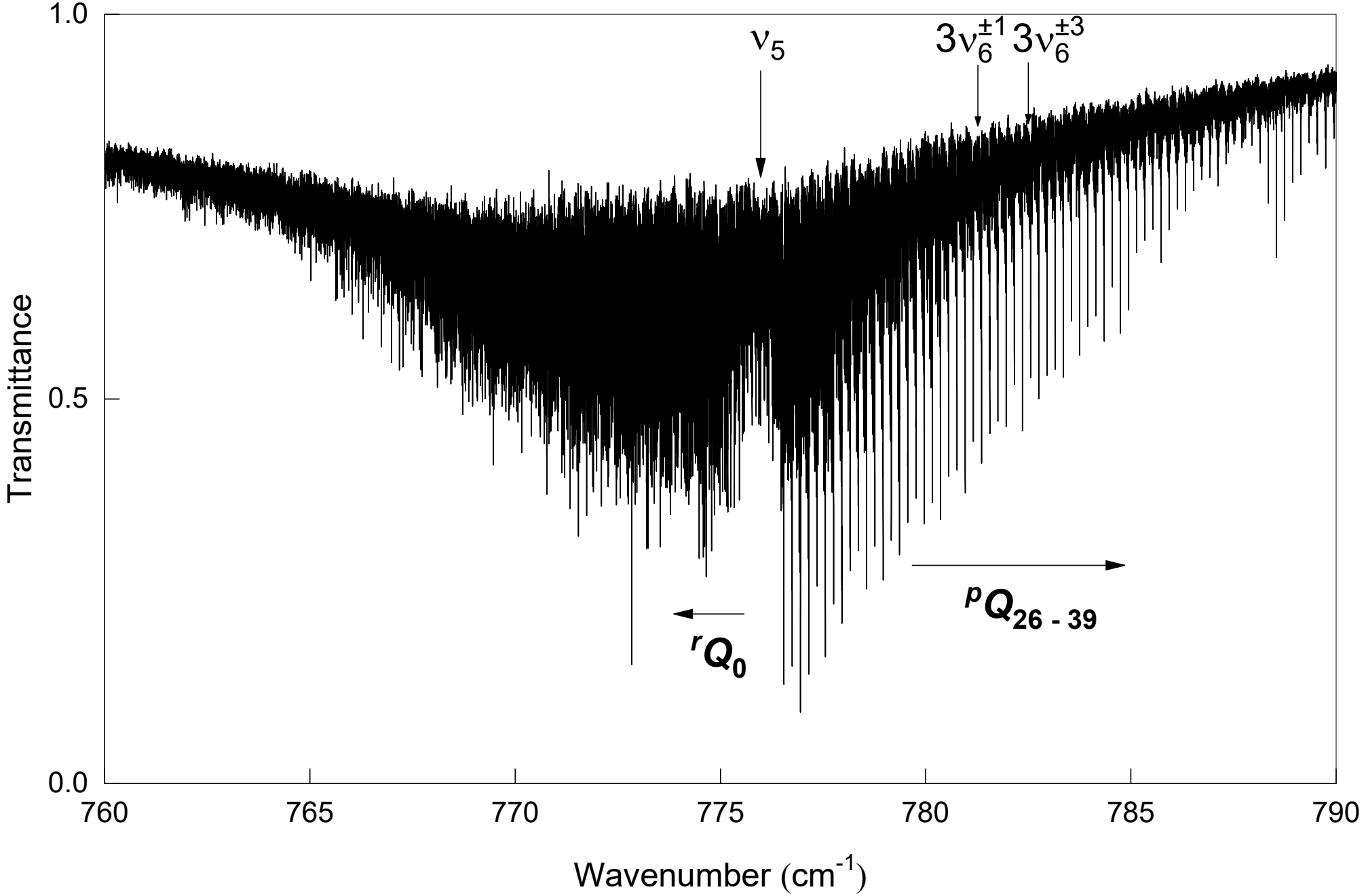
1.0
0.5
0.0
Transmittance
760
765
770
775
780
785
790
Wavenumber (cm-1)
ν5
3ν6±1 3ν6±3
rQ0
pQ26 - 39

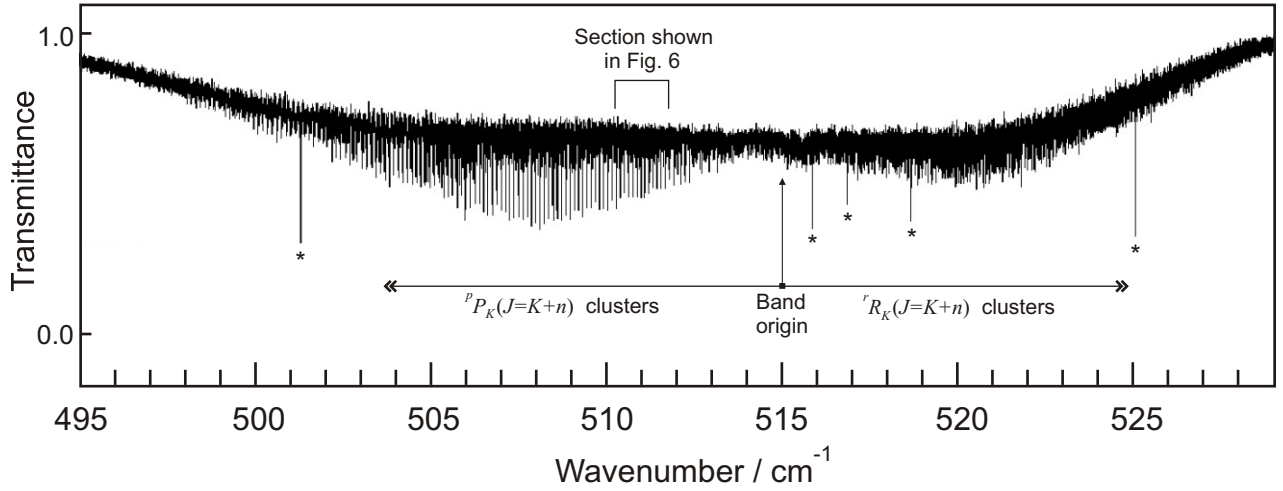
1.0
0.0
Transmittance
Section shown
in Fig. 6
*
*
*
*
*
$^{p}P_{K}(J=K+n)$ clusters
Band
origin
$^{r}R_{K}(J=K+n)$ clusters
495
500
505
510
515
520
525
Wavenumber / cm^{-1}

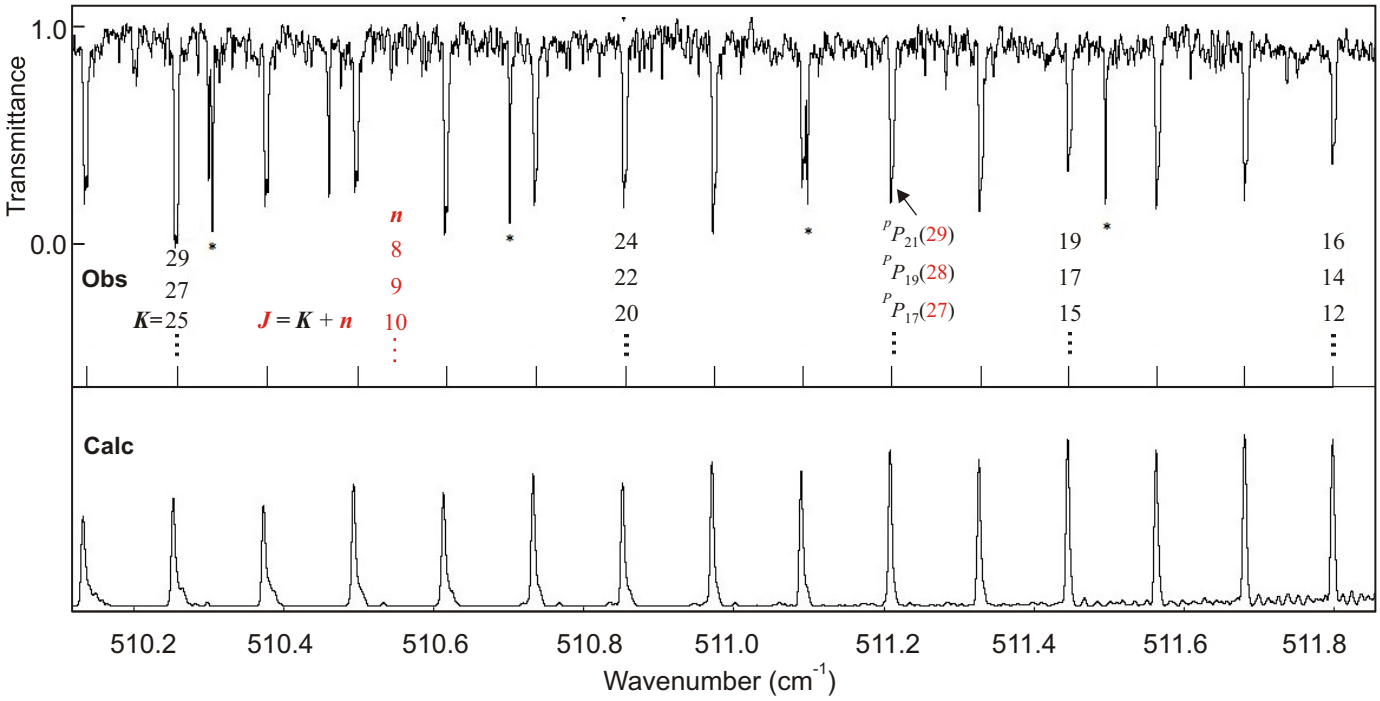
1.0
0.0
Transmittance
Obs
Calc
n
8
9
10
J = K + n
K=25
29
27
24
22
20
19
17
15
16
14
12
$^{P}P_{21}(29)$
$^{P}P_{19}(28)$
$^{P}P_{17}(27)$
510.2
510.4
510.6
510.8
511.0
511.2
511.4
511.6
511.8
Wavenumber (cm^{-1})

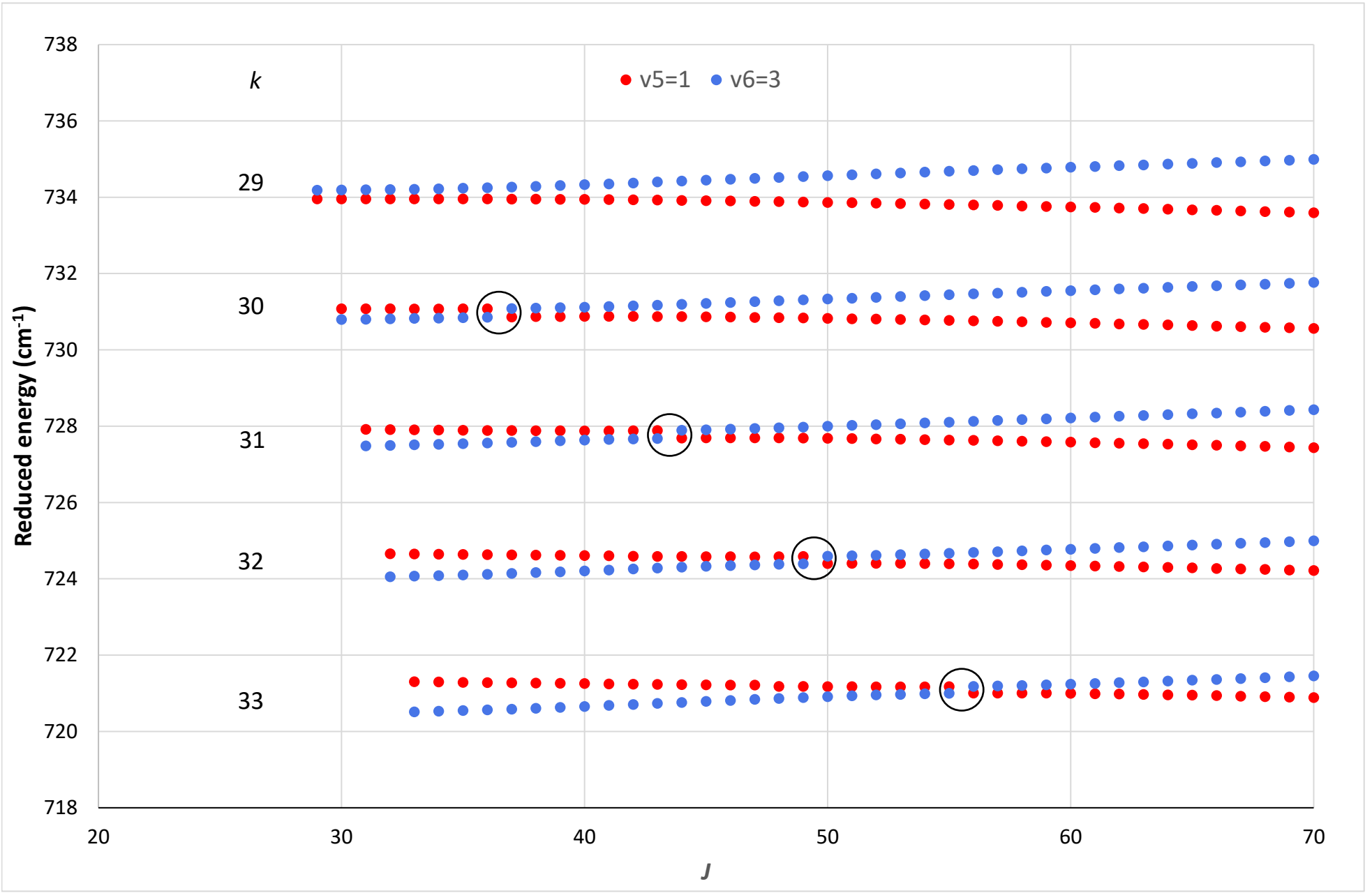
738
736
734
732
730
728
726
724
722
720
718
Reduced energy (cm-1)
k
v5=1
v6=3
29
30
31
32
33
20
30
40
50
60
70
J

Table 1. Molecular parameters of the v_2=1 and v_3=2 levels of $CH^{35}Cl_3$

Parameter	v_2=1		v_3=2, Model I
	Previous values [2]	This work	
B (MHz)	3287.259 0 (60)	3287.270 390 (99)	3297.295 13 (15)
C (MHz)	1710.254 40 (66)	1710.254 40[a]	1712.433 86[c]
D_J (kHz)	1.508 1 (25)	1.510 664 (28)	1.507 645 (62)
D_{JK} (kHz)	-2.473 (14)	-2.468 72 (45)	-2.494 75 (73)
D_K (kHz)	0.779 27 (19)	0.779 27[a]	0.825 68[b]
H_J (mHz)		1.273 2 (24)	1.290 8 (64)
H_{JK} (mHz)		-4.774 (60)	-4.29 (22)
H_{KJ} (mHz)		6.375[b]	5.494[d]
H_K (mHz)		-2.479[b]	-2.479[b]
L_J (nHz)		-2.498[b]	-2.498[b]
h_3 (mHz)		0.152 46 (82)	0.127 8 (97)
σ (kHz)		36.4	40.2

[a] Fixed to values obtained from the differences given in Ref. [2], Table 2, and the ground state values given in Ref. [14].
[b] Fixed to the corresponding ground state values, Ref. [14].
[c] Fixed to the value obtained from C_0 (Ref. [14]) and α_3^C (Ref. [4]).
[d] Fixed to the corresponding value obtained for the v_3=1 level in Ref. [9].
Numbers in parentheses are standard deviations in units of the last digit quoted.

Table 2. Molecular parameters of the v_3=2, v_5=1, and v_6=3 levels of $CH^{35}Cl_3$

Parameter	v_3=2, Model II	v_5=1	$v_6=3^{\pm1}$	$v_6=3^{\pm3}$
E (cm^{-1})	734.472 1[a]	775.964 322 9 (65)	781.622 649 (95)	782.433 902 (63)
B (MHz)	3297.424 98 (26)	3296.593 14 (17)	3306.432 79 (30)	3306.613 33 (15)
C (MHz)	1712.433 86[b]	1708.402 57 (73)	1709.179 9 (41)	1709.148 0[g]
D_J (kHz)	1.507 72 (11)	1.517 641 (81)	1.510 84 (20)	1.518 60 (20)
D_{JK} (kHz)	-2.498 5 (13)	-2.550 60 (43)	-2.516 7 (10)	-2.533 03 (85)
D_K (kHz)	0.825 68[c]	0.721 41 (37)	0.830 22 (14)	0.834 56[f]
H_J (mHz)	1.293 (11)	1.285 (12)	1.291 51[f]	1.291 51[f]
H_{JK} (mHz)	-4.31 (38)	-4.775 (80)	-5.050 42[f]	-5.050 42[f]
H_{KJ} (mHz)	5.494[d]	6.375[c]	6.333 62[f]	6.333 62[f]
H_K (mHz)	-2.479[c]	-2.479[c]	-2.434 67[f]	-2.434 67[f]
L_J (nHz)	-2.498[c]	-2.498[c]		
$C\zeta$ (MHz)		1425.633 3 (70)	-1500.424 (19)	-1500.488 32[h]
η_J (kHz)		10.487 4 (73)	-4.818 (29)	-4.938 69[f]
η_K (kHz)		-12.094 (17)	3.267 52[f]	3.267 52[f]
τ_J (Hz)		0.049 2 (17)		
τ_{JK} (Hz)		-0.172 3[e]		
τ_K (Hz)		-1.903[e]		
q_{22} (MHz)		-0.699 17 (10)	-1.828 960 (84)	
f_{22}^J (Hz)		2.633 7[e]	4.004 (39)	
f_{22}^K (Hz)			-3.066[f]	
d_t (kHz)		7.277 3 (43)		
q_{12} (MHz)			-0.072 51[i]	
q_{12}^l (MHz)			0.087 2 (17)	
f_{12}^{lJ} (Hz)			-6.541[i]	
ζ_{335} (MHz)	401.18[j]			
k_{5666} (MHz)		2429.031 (37)		

f_{41}^{a} (MHz)		-0.855 80 (60)	
f_{42}^{b} (kHz)		-1.10 (15)	
f_{42} (Hz)		-22.042 (37)	
h_3 (mHz)	0.125 (17)	0.150 1[c]	
σ^{k}	MMW: 40.2	IR: 0.237×10^{-3} MMW: 65.2	IR: 0.231×10^{-3} MMW: 43.5

[a] Constrained to the value obtained from the ν_3 and $2\nu_3 - \nu_3$ bandcenters, Ref. [4].
[b] Constrained to a value obtained from C_0 [10] and α_3^C, quoted in [4].
[c] Constrained to the corresponding GS values, Ref. [14].
[d] Constrained to the corresponding value in the v_3=1 level, Ref. [9].
[e] Constrained to values obtained in a preliminary fit.
[f] Constrained to the corresponding v_6=1 values, Ref. [14].
[g] Constrained to a value obtained from the GS and v_6=1 [14] values, and assuming a linear vibrational dependence.
[h] Constrained to a value obtained from the v_6=1 [14] and v_6=2 [1] values, and assuming a linear vibrational dependence.
[i] Constrained to the corresponding v_6=2 values, Ref. [1].
[j] Constrained to an anharmonic force field value, Ref. [17].
[k] In kHz for the MMW lines, in cm^{-1} for the IR data.
Numbers in parentheses are standard deviations in units of the last digit quoted.

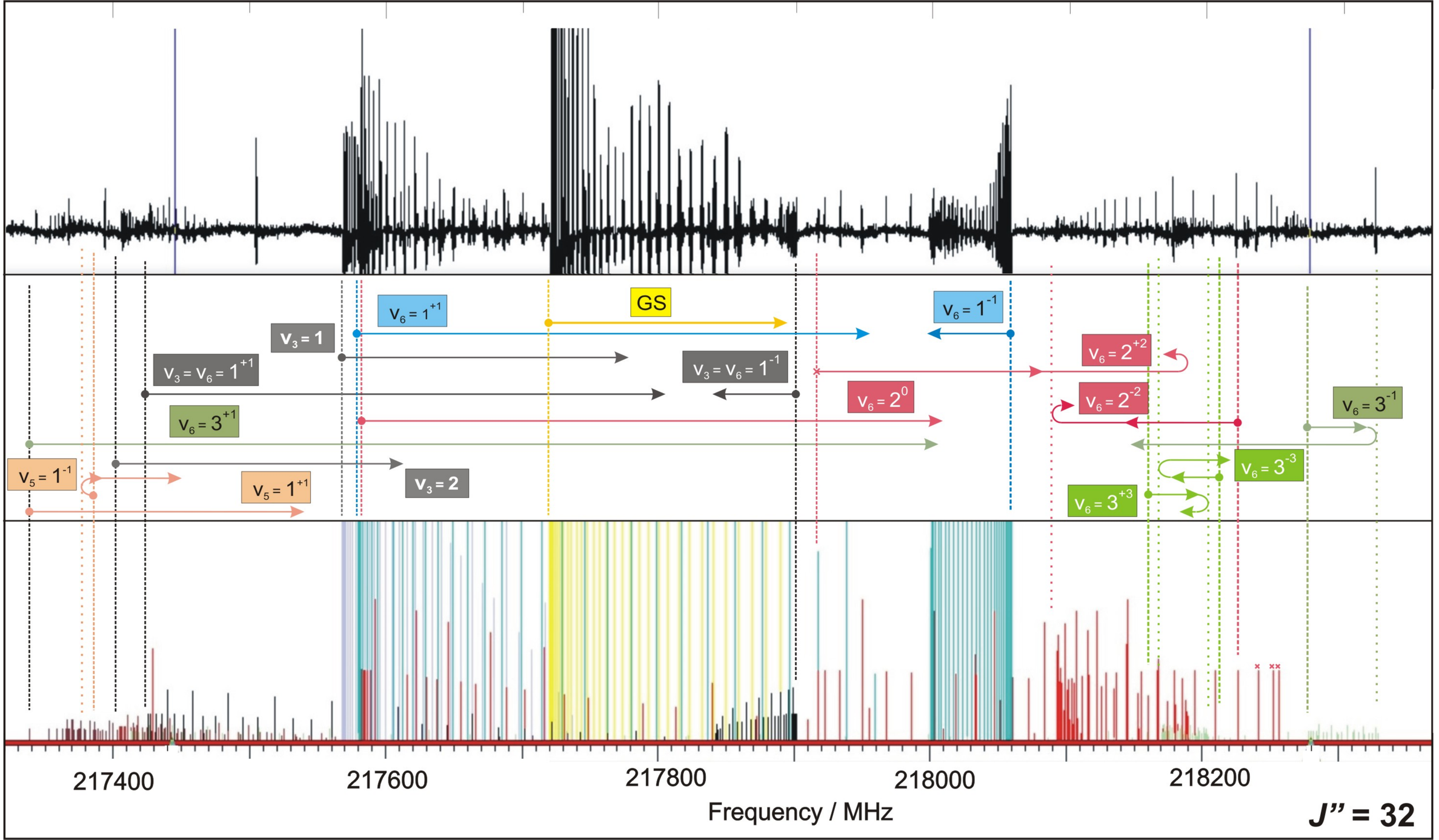
GS
$v_6 = 1^{+1}$
$v_6 = 1^{-1}$
$v_3 = 1$
$v_3 = v_6 = 1^{+1}$
$v_3 = v_6 = 1^{-1}$
$v_6 = 2^{+2}$
$v_6 = 2^{0}$
$v_6 = 2^{-2}$
$v_6 = 3^{+1}$
$v_6 = 3^{-1}$
$v_5 = 1^{-1}$
$v_5 = 1^{+1}$
$v_3 = 2$
$v_6 = 3^{-3}$
$v_6 = 3^{+3}$
217400
217600
217800
218000
218200
Frequency / MHz
J" = 32